

# Dual Lewis Acidic/Basic Pd<sub>0.5</sub>Ru<sub>0.5</sub>-Poly(*N*-vinyl-2-pyrrolidone) Alloyed Nanoparticle: Outstanding Catalytic Activity and Selectivity in Suzuki–Miyaura Cross-Coupling Reaction

Md. Shahajahan Kutubi,<sup>\*,[a, b]</sup> Katsutoshi Sato,<sup>[a, c]</sup> Kenji Wada,<sup>[d]</sup> Tomokazu Yamamoto,<sup>[b, e]</sup> Syo Matsumura,<sup>[b, e]</sup> Kohei Kusada,<sup>[b, f]</sup> Hirokazu Kobayashi,<sup>[b, f]</sup> Hiroshi Kitagawa,<sup>\*,[b, f, g, h]</sup> and Katsutoshi Nagaoka<sup>\*,[a, b]</sup>

This article anticipates the development of dual Lewis acidic/basic alloyed nanoparticle (NP) of poly(*N*-vinyl-2-pyrrolidone)-stabilized Pd<sub>0.5</sub>Ru<sub>0.5</sub> solid solution, revealing equivalent Pd<sup>δ+</sup> and Ru<sup>δ-</sup> on the NP surface. This unsupported NP disclosed excellent catalytic efficiency with high turnover frequency, 15000 h<sup>-1</sup> in Suzuki–Miyaura cross-coupling under notable drop of both Pd loading (0.08 mol%) and time (5 min) in air, attributed for its bifunctional acidic/basic modes. The bifunctional modes exposed the most interesting new reaction

mechanism ascribed by the inductive effects of *p*-substituents in arylboronic acid, accelerated reactivity by electron-withdrawing group, revealing an opposite reactivity trend relative to other Pd-based catalysts. Besides, the significant drops of Pd loading and reaction time impeded the metal leaching associated with no changes in NP surface composition/structure after the 3rd cycle (>99% efficiency), revealing a line-up for this NP in the environmental sustainability.

## Introduction

Noble-metal nanostructures have engrossed enormous interest because of their novel properties and corresponding applications in broad-range areas, such as catalysis, sensing, surface-enhanced spectroscopy, biological imaging, optoelectronics etc.<sup>[1]</sup> and catalysis has been signified as the most important chemical application of metal nanoparticles (NPs) from recent years.<sup>[1b]</sup> Among the nanostructures, bimetallic NPs have been fascinating a significant scientific and technological perspective by their distinctly different superior catalytic activity in chemical transformations over that of the corresponding component metal,<sup>[1b,2-5]</sup> and in addition, a noteworthy synergistic effect,

observed in the investigative studies on these distinctly different properties, attributes the considerable changes in both geometrical and electronic structures in bimetallic NPs.<sup>[6,7]</sup> However, the bimetallic alloyed structure among bimetallic NPs structures, such as core-shell, heterostructure etc., was found to be the most important nanocatalyst (NC) structure in numerous catalytic reactions (oxidation; reduction, hydrogenation, dehydrogenation, cross-coupling, etc.),<sup>[7,8]</sup> because of the uniformity in the homogeneous composition of both component metals and equal infirmity in charge (charge density) transfer,<sup>[9]</sup> revealing a well-defined catalytic active site for catal-

[a] Dr. M. S. Kutubi, Prof. K. Sato, Prof. K. Nagaoka  
Department of Applied Chemistry  
Oita University  
700 Dannoharu, Oita, Oita 870-1192 (Japan)  
E-mail: nagaoka@oita-u.ac.jp  
kutoubimohamado@oita-u.ac.jp

[b] Dr. M. S. Kutubi, T. Yamamoto, Prof. S. Matsumura, Prof. K. Kusada,  
Prof. H. Kobayashi, Prof. H. Kitagawa, Prof. K. Nagaoka  
CREST  
Japan Science and Technology (JST)  
4-1-8 Honcho, Kawaguchi, Saitama 332-0012 (Japan)

[c] Prof. K. Sato  
Elements Strategy Initiative for Catalysts and Batteries  
Kyoto University  
1-30 Goryo-Ohara, Nishikyoto-ku, Kyoto 615-8245 (Japan)

[d] Prof. K. Wada  
Department of Chemistry for Medicine, Faculty of Medicine  
Kagawa University  
1750-1 Ikenobe, Miki-cho, Kita-gun, Kagawa 761-0793 (Japan)

[e] T. Yamamoto, Prof. S. Matsumura  
Department of Applied Quantum Physics and Nuclear Engineering  
Kyushu University  
Motooka 744, Nishi-ku, Fukuoka 819-0395 (Japan)

[f] Prof. K. Kusada, Prof. H. Kobayashi, Prof. H. Kitagawa  
Division of Chemistry, Graduate School of Science  
Kyoto University  
Kitashirakawa-Oiwakecho, Sakyo-ku, Kyoto 606-8502 (Japan)  
E-mail: kitagawa@kuchem.kyoto-u.ac.jp

[g] Prof. H. Kitagawa  
Institute for Integrated Cell-Material Sciences (iCeMS)  
Kyoto University  
Yoshida, Sakyo-ku, Kyoto 606-8501 (Japan)

[h] Prof. H. Kitagawa  
INAMORI Frontier Research Center  
Kyushu University  
Motooka 744, Nishi-ku, Fukuoka 819-0395 (Japan)

Supporting information for this article is available on the WWW under <http://dx.doi.org/10.1002/cctc.201500758>.

ysis.<sup>[10]</sup> Thus, bimetallic alloyed NCs are now a hot research topic from both scientific and technological viewpoints,<sup>[11]</sup> because the development of highly active and selective, and durable noble NCs is vitally important for atomically utilizing the catalysts and the reactants with the maximum product output at low cost and low environment impact in the chemical transformation.<sup>[12]</sup> However, it is still difficult to synthesize bimetallic alloyed solid-solution NPs of uniformly homogeneous composition with predetermined shape and composition by wet chemical synthesis because of the variations in the standard reduction potential of individual alloyed metallic component, associated different atomic sizes, and reduction rates.<sup>[8,13]</sup> For example, a miscible solid solution in binary form, e.g., Ru–Rh, Rh–Pd, and Ru–Pd, is very difficult to synthesize,<sup>[14]</sup> although Ru, Rh, and Pd are neighboring 4d-series noble metals in the periodic table. Recently Kitagawa and co-workers have successfully synthesized a bimetallic Ag<sub>0.5</sub>Rh<sub>0.5</sub> alloyed NPs in uniform and homogeneous composition of both Ag and Rh.<sup>[15a]</sup> Very recently our group Kusada et al. successfully synthesized uniform and homogeneous alloyed NPs of PVP (PVP: poly(*N*-vinyl-2-pyrrolidone))-stabilized Pd<sub>x</sub>Ru<sub>1-x</sub> (Pd<sub>x</sub>Ru<sub>1-x</sub>-PVP) solid solution through a chemical reduction of metal cations by overcoming scientifically and technologically challenging barriers of different redox potentials of Pd and Ru,<sup>[15b,16]</sup> and then observed a higher catalytic activity of Pd<sub>0.5</sub>Ru<sub>0.5</sub>-PVP NPs in CO oxidation than with a usual catalyst.<sup>[15b]</sup> In addition, Wu et al. and Huang et al. reported Pd<sub>0.6</sub>Ru<sub>0.4</sub>/C NPs for formic acid electrooxidation and PdRu/MSN (MSN: mesoporous silica nanoparticles) for phenol hydrogenation separately.<sup>[16,17]</sup> However, only few of numerous Pd-based bimetallic NPs were applied to cross-coupling reactions so far.<sup>[7a,4b,12,18]</sup> although Pd-based catalysts have become a hot topic because of excellent catalytic performance in C–C cross-couplings, for example, Suzuki–Miyaura, Heck, Sonogashira etc. reactions in organic synthesis.<sup>[7,19]</sup> To the best of our knowledge, unsupported bimetallic alloyed NCs<sup>[12,18a]</sup> are very limited, although several supported bimetallic NCs were reported on cross-coupling.<sup>[7,4b,20]</sup> However, supporting materials clearly impede the evaluation of the basic and essential properties of the NP surface without the effect of metal–support interaction and therefore more uniform particle sizes cannot be obtained.<sup>[1b]</sup> In addition, the supporting material can change the original surface criteria of NPs, and different catalytic activities of the same NP supported on different materials were observed in the Suzuki–Miyaura cross-coupling (SMC) reaction by Choi and co-workers,<sup>[4b,20]</sup> for example, catalytic efficiency decreases in the order: Pd–Ag/ZnO > Pd–Cu/ZnO<sup>[20b]</sup> and Pd–Cu/C > Pd–Ag/C.<sup>[4b]</sup> However, PdRu NPs have yet not been applied for cross-coupling reaction. Herein, we further applied unsupported Pd<sub>0.5</sub>Ru<sub>0.5</sub>-PVP NPs to cross-coupling reactions to evaluate the catalytic proficiency in organic synthesis and SMC reaction was tested as a model reaction. As the catalytic performance of the NPs catalyst is largely dependent on the nanostructures, processing technologies, and the intrinsic physical and chemical properties of the constitutive components in the nanostructures,<sup>[7b]</sup> and the more important possible synergetic catalytic effect in nanocomposite catalysts is prevailed in many nanocomposites mostly synthesized by

chemical processes,<sup>[7b,19d,21]</sup> we first synthesized Pd<sub>0.5</sub>Ru<sub>0.5</sub>-PVP NPs in chemical reduction process<sup>[15b]</sup> and then characterized the NP surface. After that, NP was tested in SMC reaction with the aim of achieving considerable reduction of both Pd loading and reaction time to overcome the current metal-leaching issue<sup>[12,22]</sup> toward the development of environmentally benign bifunctional catalysts regarding greener perception, and subsequently its catalytic mechanism for C–C cross coupling reaction, as bimetallic nanoparticles are expected to reduce the cost of catalysts and improve their resistance to poisoning.<sup>[19a]</sup>

In this article, we, for the first time, focus on the new development of a robust dual Lewis acid/base characteristic NC of unsupported PVP-stabilized Pd<sub>0.5</sub>Ru<sub>0.5</sub> solid-solution NPs, which revealed uniformity and homogeneity in composition of both Pd and Ru at the atomic level and equally opposite charges (both  $\delta+$  and  $\delta-$ ) on its surface, and showed its bifunctional catalytic activity revealing high catalytic efficiency and selectivity with recycle ability in SMC reaction under mild conditions in air without structural change and metal leaching.

## Results and Discussion

### Characterization of Pd<sub>0.5</sub>Ru<sub>0.5</sub>-PVP NPs

At first, our synthesized Pd<sub>0.5</sub>Ru<sub>0.5</sub>-PVP NPs were characterized by high-resolution transmission electron microscopy (HRTEM), high-angle annular dark-field (HAADF) scanning transmission electron microscopy (STEM), and energy dispersive X-ray spectroscopy (EDS) mapping and linescan analysis, X-ray photoelectron spectroscopy (XPS) and X-ray diffraction (XRD) spectroscopy, and in addition, after the 3rd cycle of SMC reaction, this used catalyst was characterized to investigate broadly its catalytic mode in SMC reaction. The experimental results of HRTEM, HAADF-STEM, EDS mapping, and linescan analysis for fresh Pd<sub>0.5</sub>Ru<sub>0.5</sub>-PVP shown in Figure S1 in the Supporting Information revealed Pd<sub>0.5</sub>Ru<sub>0.5</sub>-PVP alloyed solid solution with homogeneous composition of both Pd and Ru at the atomic level throughout the whole crystalline Pd<sub>0.5</sub>Ru<sub>0.5</sub>-PVP NPs correlated to the previous results reported by our group.<sup>[15b]</sup>

As the XPS method is recognized as informative enough for understanding the catalytic properties of bimetallic NPs, which are dominated mainly by the metal composition and structure of the nanoparticle surface,<sup>[1b]</sup> Pd<sub>0.5</sub>Ru<sub>0.5</sub>-PVP NP surface was also characterized by XPS. The XPS results of fresh Pd<sub>0.5</sub>Ru<sub>0.5</sub>-PVP NP are shown in Figures S2(a) and S2(b) and Table 1.

**Table 1.** Core-level XPS data of Pd 3d and Ru 3p for fresh nanoparticles of Pd–PVP, Pd<sub>0.5</sub>Ru<sub>0.5</sub>-PVP and Ru–PVP.

Sample <sup>[a]</sup>	Pd 3d <sub>5/2</sub> [eV] (top peak)	Ru 3p <sub>3/2</sub> [eV] (top peak)	$\delta_{\text{Pd}}$ or $\delta_{\text{Ru}}$ [eV] (assigned)
Pd–PVP	334.30		0.0 (Pd <sup>0</sup> )
Pd <sub>0.5</sub> Ru <sub>0.5</sub> -PVP	334.55		+0.25 (Pd <sup>δ+</sup> )
Ru–PVP		461.4	0.0 (Ru <sup>0</sup> )
Pd <sub>0.5</sub> Ru <sub>0.5</sub> -PVP		460.6	–0.80 (Ru <sup>δ-</sup> )

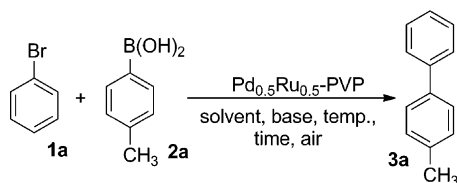
[a] PVP in all cases was 13.5 ± 0.5 wt %.

These results revealed the binding energy shift positively in Pd 3d<sub>5/2</sub> and negatively in Ru 3p<sub>3/2</sub> relative to those in individual monometal Pd–PVP and Ru–PVP. These results predicted the surface electronic structure of fresh Pd<sub>0.5</sub>Ru<sub>0.5</sub>–PVP NPs clearly correlated to the results in earlier article.<sup>[15b]</sup> The binding energy shifts, which were positively in Pd 3d and negative in Ru 3p, addressed somewhat oxidation on Pd by +0.25 eV, assuming the developing of partial positive charge ( $\delta^+$ ), and somewhat reduction in Ru by –0.8 eV, growing partial negative charge ( $\delta^-$ ) in Pd<sub>0.5</sub>Ru<sub>0.5</sub>–PVP NP surface for electron-density transfer from the fully occupied 4d orbital of Pd (Pd(46) = [Kr]4d<sup>10</sup>) toward the partially filled 4d orbital of Ru (Ru(44) = [Kr]4d<sup>7</sup>5s<sup>1</sup>).<sup>[23,24]</sup>

In addition, these results of XPS experiments also support the d-band theory (recently developed), which reveals a significant role of electronic and geometric properties of NCs with their catalytic performance<sup>[25]</sup> exploring the generation of a new electronic state during bimetallic alloy formation by hybridization of valence shell orbitals of component metals and, consequently, a flow of charge density (d electrons and d holes (d-band center)) towards the metal of partially unoccupied valence orbitals from the metal of fully occupied valence orbitals (valence bands).<sup>[26,27]</sup> Therefore, the uniform distribution of both  $\delta^+$  on Pd and  $\delta^-$  on Ru are attributed to the Pd<sub>0.5</sub>Ru<sub>0.5</sub>–PVP NPs surface assigning Pd <sup>$\delta^+$</sup> Ru <sup>$\delta^-$</sup> (1:1)–PVP NPs. For simplicity, Pd<sub>0.5</sub>Ru<sub>0.5</sub>–PVP stands for Pd <sup>$\delta^+$</sup> Ru <sup>$\delta^-$</sup> (1:1)–PVP throughout this article.

### Pd<sub>0.5</sub>Ru<sub>0.5</sub>–PVP NPs-catalyzed SMC Reaction

Evaluation of the catalytic efficiency of the Pd<sub>0.5</sub>Ru<sub>0.5</sub>–PVP NPs catalyst was first performed by optimizing the condition of the SMC reaction between bromobenzene (**1a**) and 4-methylphenylboronic acid (**2a**) in Scheme 1 under the screening of different amounts of both substrates (**1a** and **2a**) and catalyst (Pd<sub>0.5</sub>Ru<sub>0.5</sub>–PVP NPs), different bases (Na<sub>2</sub>CO<sub>3</sub>, K<sub>2</sub>CO<sub>3</sub>, Rb<sub>2</sub>CO<sub>3</sub>, Cs<sub>2</sub>CO<sub>3</sub>, NaOAc, KSCN, (NH<sub>4</sub>)<sub>2</sub>HPO<sub>4</sub>, and Na<sub>2</sub>HPO<sub>4</sub>), different solvents (toluene, CH<sub>3</sub>CN, ethanol, 1,4-dioxane, DMA (*N,N*-dimethylacetamide), DMF (*N,N*-dimethylformamide), 1,2-dimethoxyethane, and water) in either single or binary system with H<sub>2</sub>O) by stirring at a different temperature for a different time in air, regarding very high efficiency and selectivity with a significant reduction in both metal loading and reaction time in greener perception. The experimental results were tabulated in the Tables S1–S3 in the Supporting Information. This study summarized the optimized conditions of 1.0 mmol **1a** with 1.2 mmol **2a** in the presence of 0.16 mol% Pd<sub>0.5</sub>Ru<sub>0.5</sub>–PVP NPs and



**Scheme 1.** Pd<sub>0.5</sub>Ru<sub>0.5</sub>–PVP NPs-catalyzed SMC reaction between bromobenzene (**1a**) and 4-methylphenylboronic acid (**2a**) for the optimization of the reaction conditions.

3 mmol K<sub>2</sub>CO<sub>3</sub> in 6 mL DMA/H<sub>2</sub>O (1:1) system at 100 °C for 5 min stirring in air, affording product **3a** in 98% (isolated) with >99% selectivity (entry 1 in Table 3).

To investigate the surface criteria of Pd<sub>x</sub>Ru<sub>1-x</sub>–PVP ( $x = 0.0 - 1.0$ ) NPs with different composition in Pd and Ru, Pd<sub>x</sub>Ru<sub>1-x</sub>–PVP NPs and Pd salts (PdCl<sub>2</sub> and Pd(CH<sub>3</sub>CO<sub>2</sub>)<sub>2</sub>) were screened for the reaction in Scheme 1 under optimized conditions (except for the catalyst), and the corresponding results are listed in Table 2. Here Pd<sub>0.5</sub>Ru<sub>0.5</sub>–PVP NPs afforded the highest efficiency, yielding >99% **3a** (entry 6), whereas, monometallic Ru<sup>0</sup>–PVP NPs did not show any catalytic performance, even at a higher amount (3 times the amount in entry 6) of catalyst loading (entries 1, 2), although only Na et al. found efficient catalysis of 5 mol% Ru–PVP NP supported on Al<sub>2</sub>O<sub>3</sub> at 90 °C for 12 h reaction time.<sup>[28]</sup> Here we reduced both time (from 12 h to 5 min), and catalyst amount (Ru from 5 mol% to 0.08 mol%) relative to their developed method. However, 0.16 mol% Pd<sup>0</sup>–PVP NPs gave 39% yield of **3a** (entry 3), and a physical mixture of 0.16 mol% Pd<sup>0</sup>–PVP and 0.16 mol% Ru<sup>0</sup>–PVP gave 52% yield (and 55% yield for 0.32 mol% Ru<sup>0</sup>–PVP) of **3a** (entries 4 and 5). Such results assign the synergistic effects in bimetallic alloyed solid solution and cooperative participation of both metallic components. In addition, 0.16 mol% of each of Pd<sub>0.1</sub>Ru<sub>0.9</sub>–, Pd<sub>0.3</sub>Ru<sub>0.7</sub>–, and Pd<sub>0.7</sub>Ru<sub>0.3</sub>–PVP yielded 52%, 75%, and 70% of **3a**, respectively (entries 7–9), and 0.16 mol% of PdCl<sub>2</sub> and Pd(CH<sub>3</sub>CO<sub>2</sub>)<sub>2</sub> in homogeneous catalysis gave 29% and 65% yield of **3a** with Pd-black formation (entries 10 and 11). This study focused on the best catalytic activity of Pd<sub>0.5</sub>Ru<sub>0.5</sub>–PVP relative to other compositions in Pd<sub>x</sub>Ru<sub>1-x</sub>–PVP ( $x \neq 0.5$ ). Such outstanding catalytic activity of Pd<sub>0.5</sub>Ru<sub>0.5</sub>–PVP NC was ascribed to uniform coexistence of both opposite charges (Pd <sup>$\delta^+$</sup>  and Ru <sup>$\delta^-$</sup> ) on its surface in bifunctional modes, serving acceptor and donor properties<sup>[24]</sup> as well as dual Lewis acid/base properties at a time. The charge transfer rises somewhat of the Pd characteristics on Ru by the synergetic effect.<sup>[24]</sup> These bifunctional modes cooperatively participate in the catalysis through rapid cleavage of both the polar C <sup>$\delta^+$</sup> –X <sup>$\delta^-$</sup>  bond of Ar–X (Ar = aryl), and the polar C <sup>$\delta^-$</sup> –B <sup>$\delta^+$</sup>  bond of Ar–B(OH)<sub>2</sub>. But, in another composition, for example, either Pd > Ru or Ru > Pd in

**Table 2.** Screening of catalysts in SMC reaction (Scheme 1) under optimized conditions.

Entry	Catalyst/PVP <sup>[a]</sup> [mol%]	Size [nm]	Yield ( <b>3a</b> ) [%] <sup>[b]</sup>
1	Ru (0.16)	6.4 ± 1.7	0
2	Ru (0.5)	6.4 ± 1.7	0
3	Pd (0.16)	9.8 ± 2.6	39
4	Pd, Ru (0.16, 0.16)	mixture	52
5	Pd, Ru (0.16, 0.32)	mixture	55
6	Pd <sub>0.5</sub> Ru <sub>0.5</sub> (0.16)	10.0 ± 1.2	>99
7	Pd <sub>0.1</sub> Ru <sub>0.9</sub> (0.16)	9.4 ± 1.7	52
8	Pd <sub>0.3</sub> Ru <sub>0.7</sub> (0.16)	10.4 ± 1.9	75
9	Pd <sub>0.7</sub> Ru <sub>0.3</sub> (0.16)	8.2 ± 1.6	70
10	PdCl <sub>2</sub> (0.16)	bulk	29
11	Pd(CH <sub>3</sub> CO <sub>2</sub> ) <sub>2</sub> (0.16)	bulk	65

[a] PVP: 13.5 ± 0.5 wt %. [b] <sup>1</sup>H NMR yield based on internal standard 1,3,5-trimethoxybenzene.

$\text{Pd}_x\text{Ru}_{1-x}\text{-PVP}$  ( $x \neq 1-x$ ), opposite charges on the NP surface are not uniform and equal to each other. Therefore, the  $\text{Pd}_{0.5}\text{Ru}_{0.5}\text{-PVP}$  surface in 1:1 composition of Pd/Ru shows outstanding catalytic efficiency in SMC reaction relative to other compositions.

Encouraged by this outstanding catalytic efficiency with the particular attention to uniform  $\text{Pd}^{\delta+}$  and  $\text{Ru}^{\delta-}$  components on  $\text{Pd}_{0.5}\text{Ru}_{0.5}\text{-PVP}$  NP surface, this catalyst was also tested to investigate the role of the inductive effect by electron-donating-group (EDG) and electron-withdrawing-group (EWG) substituents, on both *p*-substituted aryl halides (**1**) and *p*-substituted arylboronic acids (**2**) in Scheme 2 under optimized conditions. The corresponding results are summarized in Table 3.

The results in Table 3 show that most of the SMC reactions afforded 97%–>99% yield with >99% selectivity except for entries 5, 9, and 10. The reactions of EDG ( $\text{CH}_3$  or  $\text{OCH}_3$ )-substituted phenyl bromides (**1c**, **1d**) with EDG ( $\text{OCH}_3$ )-substituted phenylboronic acid (**2c**) afforded relatively low yields in 70% **3c**, 78% **3d**, and 65% **3e** (entries 5, 9, and 10). Here, for *p*-substituted phenyl bromides, higher reactivity by EWG substituents



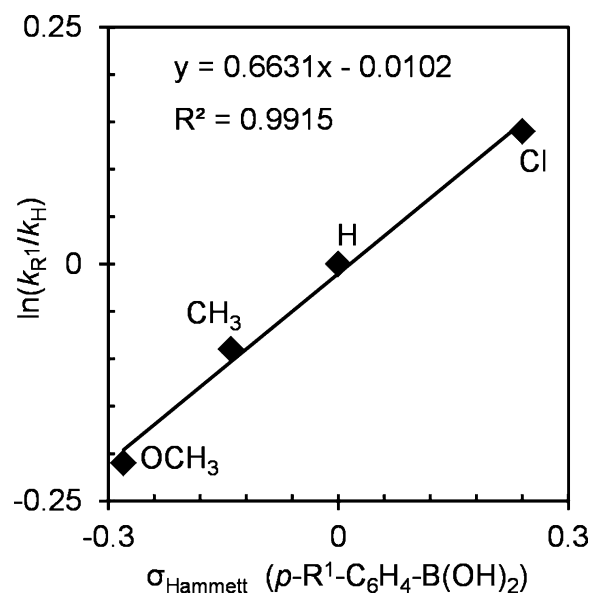
**Scheme 2.**  $\text{Pd}_{0.5}\text{Ru}_{0.5}\text{-PVP}$  NPs-catalyzed SMC reactions of aryl halide (**1**) with arylboronic acid (**2**) under optimized conditions.

Table 3. Results of substrates ( <b>1</b> and <b>2</b> ) screening in Scheme 2. <sup>[a]</sup>			
Entry	R, X ( <b>1</b> ); R <sup>1</sup> ( <b>2</b> )	Product ( <b>3</b> )	Yield <sup>[b]</sup> [%]
1	H, Br ( <b>1a</b> ); CH <sub>3</sub> ( <b>2a</b> )		98
2	H, I ( <b>1b</b> ); CH <sub>3</sub> ( <b>2a</b> )	<b>3a</b>	>99
3	CH <sub>3</sub> , Br ( <b>1c</b> ); H ( <b>2b</b> )		>99
4	CH <sub>3</sub> , Br ( <b>1c</b> ); CH <sub>3</sub> ( <b>2a</b> )	<b>3b</b>	>99
5	CH <sub>3</sub> , Br ( <b>1c</b> ); OCH <sub>3</sub> ( <b>2c</b> )		70
6	OCH <sub>3</sub> , Br ( <b>1d</b> ); CH <sub>3</sub> ( <b>2a</b> )	<b>3c</b>	97
7	OCH <sub>3</sub> , Br ( <b>1d</b> ); H ( <b>2b</b> )		99
8	H, I ( <b>1b</b> ); OCH <sub>3</sub> ( <b>2c</b> )	<b>3d</b>	>99
9	H, Br ( <b>1a</b> ); OCH <sub>3</sub> ( <b>2c</b> )		78
10	OCH <sub>3</sub> , Br ( <b>1d</b> ); OCH <sub>3</sub> ( <b>2c</b> )	<b>3e</b>	65
11	CH <sub>3</sub> CO, Br ( <b>1e</b> ); H ( <b>2b</b> )		>99
12	CH <sub>3</sub> CO, Br ( <b>1e</b> ); CH <sub>3</sub> ( <b>2a</b> )	<b>3f</b>	>99
13	CH <sub>3</sub> CO, Br ( <b>1e</b> ); OCH <sub>3</sub> ( <b>2c</b> )		>99
14	H, I ( <b>1b</b> ); H ( <b>2b</b> )		>99
15	H, Br ( <b>1a</b> ); H ( <b>2b</b> )	<b>3i</b>	98
16	H, I ( <b>1b</b> ); Cl ( <b>2d</b> )		>99

[a] Under optimized conditions. [b] Isolated yield.

and lower reactivity by EDG substituents (entries 5, 9, and 10) were observed in the reactivity trend:  $\text{H} > \text{CH}_3 > \text{OCH}_3$ , and this reactivity trend is the same as that observed in either Pd-catalyzed<sup>[29,30]</sup> or bimetallic NPs-catalyzed<sup>[12,19a]</sup> SMC reactions. Here, this is caused by inductive effects governed by the increase of electron density for EDG (or decrease for EWG) substituents in the C–X bond, making it stronger, resulting in lower reactivity (or weaker by EWG, revealing higher reactivity). However, *p*-substituted arylboronic acids, *p*-R<sup>1</sup>-C<sub>6</sub>H<sub>4</sub>B(OH)<sub>2</sub> (**2**), showed higher reactivity by EWG substituents and lower reactivity by EDG substituents, affording >99% **3a** for R<sup>1</sup>=H (**2b**) in entry 3 and 70% **3c** for R<sup>1</sup>=OCH<sub>3</sub> (**2c**) in entry 5 with the same *p*-Me-C<sub>6</sub>H<sub>4</sub>-Br (**1c**). This reactivity trend observed for **2** is absolutely opposite to that in Pd-catalyzed SMC reactions.<sup>[31,30b]</sup> Therefore, inspired by such new reactivity trend for **2**, a kinetic study for **2** regarding a variety of *p*-substituents, R<sup>1</sup>: OCH<sub>3</sub> (**2c**), CH<sub>3</sub> (**2a**), H (**2b**), and Cl (**2d**) with **1a** was investigated in Scheme S1 (Section 2.4 in the Supporting Information) to clearly elucidate the inductive effects for EWG and EDG in **2** and then kinetic results was used to sketch the familiar Hammett plots<sup>[30a,b]</sup> shown in Figure 1. The Hammett plot explored a linear correlation by higher catalytic activity for EWG and vice versa for EDG in the reactivity trend: R<sup>1</sup>=Cl > H > CH<sub>3</sub> > OCH<sub>3</sub> in **2**, and revealed negative charge built up on aromatic ring of **2** in the transition state (see the mechanism in Scheme 4), which is stabilized by EWG (and destabilized by EDG) on **2**, and subsequently the reaction rate accelerated by EWG, but slowed down by EDG.

Besides, although supported nanoparticles usually show recycle ability,<sup>[32]</sup> the recycling assessment of the unsupported  $\text{Pd}_{0.5}\text{Ru}_{0.5}\text{-PVP}$  NPs in the successive three cycles<sup>[12]</sup> (by addition of substrates base and solvents<sup>[29]</sup>) revealed >99% efficiency (>99% product **3j** in each cycle) without any loss of the catalytic activity in SMC reaction between phenyl iodide (**1b**) and 4-chlorophenylboronic acid (**2d**) under optimized conditions in



**Figure 1.** Hammett plot for  $\text{Pd}_{0.5}\text{Ru}_{0.5}\text{-PVP}$  NPs-catalyzed SMC reactions (Scheme S1).

air (see details in the Supporting Information Section 2.5 and Table S4) at the significant reduction of both Pd loading (0.08 mol%) and reaction time (5 min) focusing on very high average turnover frequency (TOF: the mole of product produced per mole Pd (total) per hour)  $15000\text{ h}^{-1}$  relative average TOF:  $\approx 3600\text{ h}^{-1}$  ( $\approx 1.0\text{ s}^{-1}$  for three cycles, calculated as the product formed per surface Pd atom per second for Pd–Rh NPs<sup>[12]</sup>), as average TOF values giving the rate of product formation measured in each cycle are valid and meaningful data.<sup>[19c,e]</sup> As consistently high conversions or yields in a few repeated runs are taken as evidence to prove the high potential of the catalyst,<sup>[19c]</sup> and change in bimetallic composition and geometrical structure during SMC reaction,<sup>[12]</sup> this used catalyst after the 3rd cycle, without further recycle experiment, was tested for the STEM–EDS mappings and linescan analysis, and XRD spectroscopy experiments to find out any change in NP surface during SMC reactions. However, some reports focused on 5–10 times recyclability, but there longer reaction times were required, resulting in very low average TOF, for example, Hoshiya et al. reported 10 recycles with 0.007 mol% Pd for supported Pd–Au NPs, each for 12 h at 80 °C in argon, revealing average TOF  $113\text{ h}^{-1}$ <sup>[22a]</sup> ( $\approx 1/133$  of that observed in Pd<sub>0.5</sub>Ru<sub>0.5</sub>–PVP NPs).

Here, the experimental results of STEM–EDS mappings and linescan analyses, and XRD spectroscopy for used Pd<sub>0.5</sub>Ru<sub>0.5</sub>–PVP NC after 3rd cycle shown in Figures 2, and S3 separately revealed the existence of a uniform homogeneous solid solution of both Pd and Ru without any changes in both i) uniform bimetallic composition of Pd and Ru in solid solution alloyed NPs and ii) geometrical structure in Pd<sub>0.5</sub>Ru<sub>0.5</sub>–PVP NPs after 3rd cycle of SMC reaction, compared with those of fresh Pd<sub>0.5</sub>Ru<sub>0.5</sub>–PVP NPs (Figures S1 and S3). Such result of unchanging in the bimetallic composition and structural geometry explored no displacement of compositional metals (Pd and Ru) in the alloyed Pd<sub>0.5</sub>Ru<sub>0.5</sub>–PVP NPs during the SMC reaction and therefore, no metal leaching occurred, whereas recently Wang and co-workers reported the changes in shape and surface structure of bimetallic Pd–Rh nanocrystal associated with metal leaching (5–15% of original amount of catalyst found by inductively coupled plasma atomic emission spectroscopy (ICP–AES) in SMC reaction.<sup>[12]</sup>

Moreover, to clarify the metal leaching in Pd<sub>0.5</sub>Ru<sub>0.5</sub>–PVP NPs catalysis, at first, the SMC reaction between **1a** and **2a** Scheme 1 (see also Supporting Information Section 2.6), performed under optimized conditions (or in 6 mL EtOH/H<sub>2</sub>O (1:1) at 30 °C for 10 min in air) for the three catalysts Pd<sub>0.5</sub>Ru<sub>0.5</sub>–PVP NPs, Pd–PVP NPs and homogeneous Pd(CH<sub>3</sub>CO<sub>2</sub>)<sub>2</sub>, separately for the original catalytic activity test and then leached metal activity test for each catalyst, was performed for additional 3 h described in detail in the Supporting Information Section 2.6. The results are shown in Tables S5 and S6. The leached metal activity test revealed additional yields of **3a** of 0% for Pd<sub>0.5</sub>Ru<sub>0.5</sub>–PVP at both 100 °C and 30 °C, respectively, and 5% and 35% for Pd–PVP NPs and homogeneous Pd(CH<sub>3</sub>CO<sub>2</sub>)<sub>2</sub> at 100 °C, respectively, (but 0% and 79% yield of **3a**, respectively, at 30 °C). Besides, ICP–AES analysis of the residual water part collected after separation of the organic part confirmed no

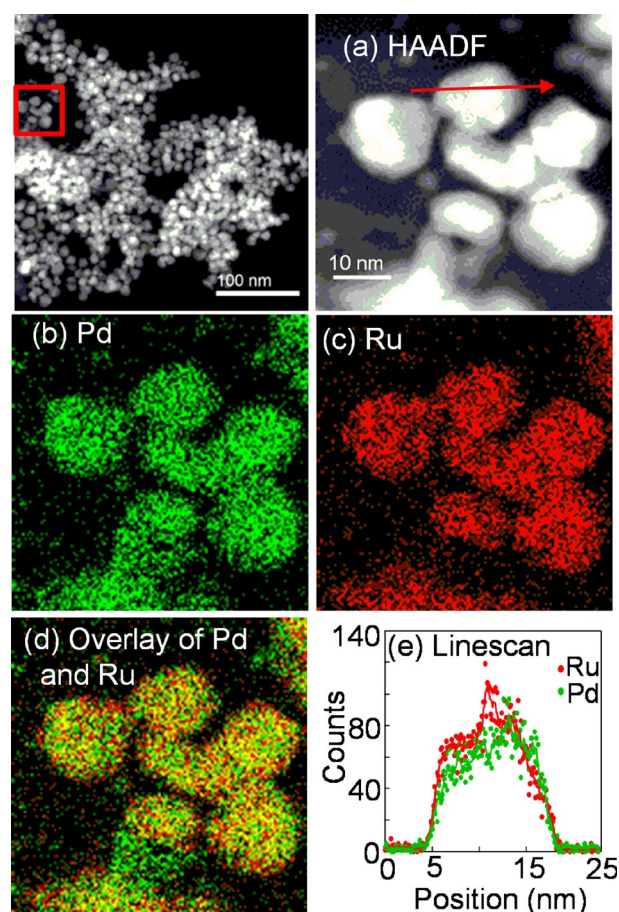


**Figure 2.** HAADF–STEM image of Pd<sub>0.5</sub>Ru<sub>0.5</sub>–PVP NPs after the third cycle in the SMC reaction and TEM–EDS analyses of the region marked by a red box. a) HAADF–STEM image; b–d) EDS maps for Pd, Ru, and overlay of both Pd (green) and Ru (red), respectively; e) compositional linescan profile along the arrow in (a) (Pd: green and Ru: red).

leached metal detected. Thus both experimental results observed in STEM–EDS mappings and linescan analyses (Figure 2), and XRD pattern (Figure S3) correlated with the results of the leaching test. Therefore, we concluded that no metal (Pd and/or Ru) leaching was caused for the cooperative catalysis by Pd<sup>δ+</sup>–Ru<sup>δ-</sup> NPs, which possess a stronger polar covalent bond impeding the metal leaching in very short time reaction than monometallic or nonalloyed core–shell bimetallic NCs, in which only one metal participates in activating the C–X and C–B bonds for cleavage, resulting longer reaction time.<sup>[19d,22,32]</sup>

On the other hand, any homocoupling products of either aryl halide or arylboronic acid were not observed under optimized conditions. Besides, experiments with only single substrates of either **2a** or **1a** did not show any corresponding homocoupling product under optimized conditions. Therefore, it was concluded that the very low amount of catalyst and the very short reaction time were the actual reason for no homocoupling, although several studies reported somewhat homocoupling product formation during SMC reaction at low Pd loadings with long reaction time (0.09 mol% Pd, 24 h)<sup>[29]</sup> and high Pd loading with long reaction time (0.5 mol% Pd, 6 h).<sup>[33]</sup>

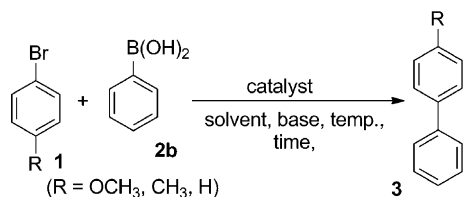
**Table 4.** Comparative catalytic efficiency in terms of TOF between Pd<sub>0.5</sub>Ru<sub>0.5</sub>-PVP NPs and other catalysts developed very recently for SMC Reaction.

Catalyst [mol% of Pd]	R (1)	t [min]	TOF [h <sup>-1</sup> ]
Pd <sub>0.5</sub> Ru <sub>0.5</sub> -PVP NPs (0.08) <sup>[a]</sup>	CH <sub>3</sub> (1 c)	5	15000
Pd <sub>0.5</sub> Ru <sub>0.5</sub> -PVP NPs(0.08) <sup>[a]</sup>	OCH <sub>3</sub> (1 d)	5	14850
Poly(imidazole-Pd) (0.004) <sup>[b]</sup>	OCH <sub>3</sub> (1 d)	180	8166 <sup>[34a]</sup>
Graphene-Ni/Pd NPs (0.91) <sup>[c]</sup>	H (1 a)	30	171 <sup>[32c]</sup>
Pd,Rh <sub>1-x</sub> nanocrystal (0.002) <sup>[d]</sup>	CH <sub>3</sub> (1 c)	20	max. ≈ 2880 <sup>[12]</sup>
Pd-PVP NPs (0.006) <sup>[e]</sup>	H (1 a)	24 h	688 <sup>[34b]</sup>

[a] Conditions (this work): 1 mmol 1 c (or 1 d), 1.2 mmol 2 b, 3 mmol K<sub>2</sub>CO<sub>3</sub>, 6 mL DMA/H<sub>2</sub>O(1:1), 100 °C. [b] Conditions:<sup>[34a]</sup> 0.5 mmol 1 c (or 1 d), 0.6 mmol 2 b, 2 mmol K<sub>2</sub>CO<sub>3</sub>, 1 mol TBAF (additive), 1.5 mL H<sub>2</sub>O, 100 °C; [c] Conditions:<sup>[32c]</sup> 2.0 mmol 1 a, 0.82 mmol 2 b, 2 equiv K<sub>2</sub>CO<sub>3</sub>, 10 mL DMF/H<sub>2</sub>O(7:3), 110 °C. [d] Conditions:<sup>[12]</sup> 0.3 mmol 1 c, 0.6 mmol 2 b, 1 mmol K<sub>2</sub>CO<sub>3</sub>, 4 mL EtOH, 85 °C. [e] Conditions:<sup>[34b]</sup> 0.5 mmol 1 a, 0.75 mmol 2 b, 1.5 mmol K<sub>3</sub>PO<sub>4</sub>, 4 mL EtOH/H<sub>2</sub>O (1:3), 90 °C.

As SMC reaction is one of the most industrially applicable organic synthesis reactions, numerous catalytic systems (both homogeneous and heterogeneous) were developed, and this is still of interest to researchers because of the universal issue of metal leaching in both homogeneous and heterogeneous catalysis, including the global industrial voice of “faster, better, and cheaper.” In Table 4, comparative catalytic efficiencies are presented in terms of TOF (based on total Pd) between Pd<sub>0.5</sub>Ru<sub>0.5</sub>-PVP NPs catalyst and other catalysts: poly(imidazole)-Pd,<sup>[34a]</sup> graphene-Ni/Pd NPs,<sup>[32c]</sup> Pd-Rh nanocrystal,<sup>[12]</sup> and PVP-stabilized Pd NPs<sup>[34b]</sup> developed by Yamada et al., 2012,<sup>[34a]</sup> Metin et al., 2012,<sup>[32c]</sup> Wang et al., 2014,<sup>[12]</sup> and Uberman et al., 2012<sup>[34b]</sup>, individually reported earlier (for SMC reaction in Scheme 3).

The results in Table 4 reveal very high efficiency and selectivity of the Pd<sub>0.5</sub>Ru<sub>0.5</sub> catalyst in the SMC reaction with higher TOF of 15000 h<sup>-1</sup> compared with those of other catalysts, poly(imidazole)-Pd: 8166 h<sup>-1</sup>, graphene-Ni/Pd NP: 171 h<sup>-1</sup>, Pd-Rh nanocrystal: 2880 h<sup>-1</sup>, and PVP-stabilized Pd NP: 688 h<sup>-1</sup>, for the same SMC reactions involving the same substrates 1 and 2b. In the case of poly(imidazole)-Pd, large amounts (2 equiv.) of expensive *n*Bu<sub>4</sub>NF (tetra-*n*-butylammonium fluoride) as an additive along with 2 equivalents of K<sub>2</sub>CO<sub>3</sub> seemed to be essential to activate the catalyst for high TOF of 8166 h<sup>-1</sup>,<sup>[34a]</sup> but Pd<sub>0.5</sub>Ru<sub>0.5</sub>-PVP NPs revealed very high TOF without such additive. Therefore, compared to Pd-based catalysts, Pd<sub>0.5</sub>Ru<sub>0.5</sub>-PVP NC revealed very high catalytic activity at the reduction of both Pd loading and reaction time, resulting in the prevention of metal leaching accompanied with no changes in bimetallic composition and geometrical structure, although other reports



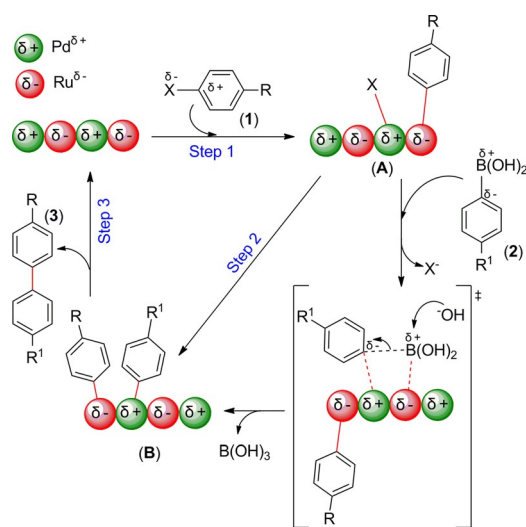
**Scheme 3.** SMC reaction for comparing the catalytic efficiencies of different catalysts.

showed somewhat high catalytic activity at either low Pd loading with longer reaction time or high Pd loading with short reaction time, associating metal leaching.

In addition, the Pd<sub>0.5</sub>Ru<sub>0.5</sub>-PVP-catalyzed SMC reaction showed the same efficiency with the same TOF of 15000 h<sup>-1</sup> under 3 or 5 times of both substrates (3 or 5 mmol) and catalyst loading (0.6 or 1.0 mg) compared with optimized conditions (1 mmol substrate and 0.2 mg catalyst) and after two years in air. This reveals a high stability of this catalyst in normal atmosphere without any loss of its catalytic activity.

As a number of researchers insisted that the Suzuki and Heck reactions would proceed at the surface of Pd-based NPs in truly heterogeneous reactions,<sup>[7b]</sup> all our results, that is, Pd<sup>δ+</sup>Ru<sup>δ-</sup> on the NP surface, no change in NP composition and structural geometry, and no metal leaching for Pd<sub>0.5</sub>Ru<sub>0.5</sub>-PVP NP catalysis in SMC reactions, attributed to a truly heterogeneous catalytic mode.<sup>[7b,12,32a]</sup> Therefore, we ascribed the following reaction mechanism (shown in Scheme 4) for the SMC reaction in Scheme 2.

In Scheme 4, step 1 involves the interaction between 1 and catalyst surface by chemisorption, affording species A (*p*-R-C<sub>6</sub>H<sub>4</sub>-cat.-X) through the rapid cleavage of C<sup>δ+</sup>-X<sup>δ-</sup> bond by cooperative participation of both Pd<sup>δ+</sup> and Ru<sup>δ-</sup>. In the presence of water, KOH (K<sub>2</sub>CO<sub>3</sub> + H<sub>2</sub>O ⇌ KOH + KHCO<sub>3</sub>) is usually formed because the SMC reaction did not proceed at all in the absence of base. Therefore, in step 2, reactant 2 interacts with species A by Pd<sup>δ+</sup> with C<sup>δ-</sup> and Ru<sup>δ-</sup> with B<sup>δ+</sup> through a transition state developing negative charge on the aromatic ring of 2 (supported by the Hammett plot, Figure 1), promoted by OH<sup>-</sup> for rapid cleavage of the C<sup>δ-</sup>-B<sup>δ+</sup> bond, and B(OH)<sub>3</sub> leaves, and finally species B is formed. This species B at step 3 rapidly undergoes associative chemisorption between the Lewis acid characteristics of the aryl part of 1 having a positive charge and the Lewis basic characteristics of the aryl part of 2



**Scheme 4.** Plausible mechanism for Pd<sub>0.5</sub>Ru<sub>0.5</sub>-PVP NPs-catalyzed SMC reaction.

having a negative charge in the manner of Lewis acid–base interaction, and subsequently biaryl product **3** is afforded followed by leaving Pd<sub>0.5</sub>Ru<sub>0.5</sub>–PVP NP for the next catalytic cycle. Here step 2 was assumed to play a significant role over the whole catalytic cycle, associating the significant transition state with negatively charged aromatic ring, correlated by the kinetic study of the Hammett plot. Therefore, step 2 was ascribed as the rate-determining step (RDS) here, conversely to the oxidative addition step as RDS<sup>[7b,35]</sup> under strongly basic support materials or ligands that lead to higher electron density on the Pd-based catalyst surface and accelerate the oxidative addition<sup>[7b]</sup> because electron-deficient Pd<sup>δ+</sup> impedes oxidative addition in Pd<sub>0.5</sub>Ru<sub>0.5</sub>–PVP NPs catalysis.

## Conclusions

We have demonstrated anomalous behavior of bimetallic Pd<sub>0.5</sub>Ru<sub>0.5</sub>–PVP (poly(*N*-vinyl-2-pyrrolidone)-stabilized Pd<sub>0.5</sub>Ru<sub>0.5</sub>) solid solution nanocatalyst in the Suzuki–Miyaura cross-coupling (SMC) reaction, revealing very high efficiency with excellent recyclability under the significant reduction of both Pd loading and reaction time without inert atmosphere. The most important findings are that this alloyed nanoparticle surface contains uniformly Pd<sup>δ+</sup> and Ru<sup>δ-</sup>, which attributes bifunctional catalytic activity in dual Lewis acidic/basic modes, and the reaction mechanism likely is completely different from that of the conventional Pd-based catalyzed SMC reaction, which is usually described in terms a single Pd metal associating the oxidative addition as rate-determining step, whereas here the transmetalation-type step is ascribed as rate-determining step regarding the transition state with negatively charged aromatic ring. The fruitful impeding of metal leaching attributed to no changes in NP surface composition/geometrical structure and a significant drop in Pd loading and reaction time would make this catalyst as a footprint in the environmental sustainability regarding a novel strategy of interelemental fusion to create highly efficient functional materials for the material conversions in organic synthesis. We believe that this development with the arguments presented hopefully makes Pd<sub>0.5</sub>Ru<sub>0.5</sub>–PVP an attractive nanocatalyst to open new possibilities for large-scale application in other cross-coupling reactions as well as chemical transformation.

## Experimental Section

### General

All manipulations were performed under normal atmospheric conditions unless otherwise noted. Reagents and solvents were purchased from commercial suppliers (Wako Pure Chemical Industries, Ltd., Japan; Tokyo Chemical Industry, TCI, Japan and Sigma Aldrich, Japan) and used without further purification. Water was deionized with a Millipore system as a Milli-Q grade. <sup>1</sup>H NMR (400 MHz) and <sup>13</sup>C NMR (100 MHz) spectra were recorded on a Bruker-400 NMR-spectrometer. Chemical shifts (δ) in <sup>1</sup>H and <sup>13</sup>C NMR spectroscopy were reported relative to that of tetramethylsilane (TMS, δ = 0.00 ppm) in NMR solvents (Cambridge Isotope Laboratories Inc., USA). GC–MS of individual pure product was performed on a gas

chromatograph mass spectrometer of GCMS–QP2010 Ultra SHIMADZU. Thin-layer chromatography analysis was performed on silica gel 60 F<sub>254</sub> (Merck KGaA, Germany). Column chromatography was performed on silica gel 60 of either 0.040–0.063 mm or 0.063–0.2 mm (Merck KGaA, Germany). In addition, ICP–AES was performed on a Shimadzu ICPS-8100 instrument by the chemical analysis team at RIKEN (Saitama 351–0198, Japan) for the metal leaching test.

### Synthesis of Pd<sub>x</sub>Ru<sub>1-x</sub>–PVP nanoparticles

At first the Pd<sub>0.5</sub>Ru<sub>0.5</sub>–PVP NPs were synthesized by a typical method of wet chemical reduction of metal ions under very slow addition of an aqueous solution (40 mL) of K<sub>2</sub>[PdCl<sub>4</sub>] (0.1634 g, 0.5 mmol) and RuCl<sub>3</sub>·*n*H<sub>2</sub>O (*n* = 3, 0.1311 g, 0.5 mmol) to a hot solution of PVP (molecular weight, MW ≈ 40 000; 0.444 g) in triethylene glycol (100 mL) under constant stirring at 200 °C in air; the temperature of approximately 200 °C was constantly maintained during the addition. After completing the addition, the whole solution was cooled to RT under constant stirring and then the Pd<sub>0.5</sub>Ru<sub>0.5</sub>–PVP NPs were isolated by centrifuging followed by vacuum drying overnight.<sup>[15b]</sup>

### Catalyst characterization

The synthesized Pd<sub>0.5</sub>Ru<sub>0.5</sub>–PVP alloyed NPs were characterized before (fresh) and after the SMC reaction (3rd cycle) by the analysis of (a) HRTEM, HAADF–STEM, and EDS, (b) XPS, and (c) XRD patterns. HRTEM, HAADF–STEM, and EDS analysis were performed firstly by sample preparation by dropwise placing thoroughly dispersed Pd<sub>0.5</sub>Ru<sub>0.5</sub>–PVP in ethanol onto a C-coated grid followed by drying through exposure under ambient conditions for 24 h, and then finally recording the HRTEM, HAADF–STEM, and EDS mapping data on a JEOL JEM–ARM 200F instrument operated at 120 kV. XPS experiments were performed on a Shimadzu ESCA-850 under the binding energy calibration with a reference of C1s orbital at 284.6 eV<sup>[23a]</sup> by placing the sample (sampling on a metal grid) into the chamber. XRD patterns were recorded on a MiniFlex 600 X-ray diffractometer (Rigaku, Japan) with Cu<sub>Kα</sub> radiation.

### Typical procedure for the SMC reaction of aryl halide (1) with arylboronic acid (2)

A 10 mL glass vial was charged with aryl halide (**1**, 1 mmol), arylboronic acid (**2**, 1.2 mmol), Pd<sub>0.5</sub>Ru<sub>0.5</sub>–PVP (0.2 mg, 0.0016 mmol; 0.0008 mmol Pd loaded, that is, 0.08 mol% Pd), K<sub>2</sub>CO<sub>3</sub> (3 mmol), and mixed solvent (6 mL) of DMA (3 mL) and H<sub>2</sub>O (3 mL) followed by constant stirring at 100 °C for 5 min in air. The reaction was then stopped immediately by dipping the bottom part of the reaction vial into ice cold water (0 °C). The organic part was extracted with diethyl ether (or ethyl acetate) (5 mL × 4) followed by centrifuging to collect the solid catalyst. Next, the combined organic part was dried over anhydrous Na<sub>2</sub>SO<sub>4</sub>, and concentrated under reduced pressure. The crude product was purified by silica gel flash column chromatography (hexane/ethyl acetate 19:1) to obtain the cross-coupling product, **3** and then isolated products were characterized by <sup>1</sup>H NMR, <sup>13</sup>C NMR, and GC–MS spectroscopies. The <sup>1</sup>H NMR yield was quantified by using the internal standard of 1,3,5-trimethoxybenzene.

## Acknowledgements

This work was financially supported for "Core Research for Evolutional Science and Technology (CREST)" by Japan Science and Technology Agency (JST), Japan.

**Keywords:** alloys · C–C coupling · nanoparticles · palladium · reaction mechanisms

- [1] a) Y. Hu, Y. Liu, Z. Li, Y. Sun, *Adv. Funct. Mater.* **2014**, *24*, 2828–2836; b) N. Toshima, T. Yonezawa, *New J. Chem.* **1998**, *22*, 1179–1201.
- [2] a) J. I. He, I. Ichinose, T. Kunitake, A. Nako, Y. Shirashi, N. Toshima, *J. Am. Chem. Soc.* **2003**, *125*, 11034–11040; b) J. M. Thomas, B. F. G. Johnson, R. Raja, G. Sankar, P. A. Midgley, *Acc. Chem. Res.* **2003**, *36*, 20–30.
- [3] a) P. V. Kamat, *J. Phys. Chem. B* **2002**, *106*, 7729–7744; b) S. Sun, C. B. Murray, D. Weller, L. Folks, A. Moser, *Science* **2000**, *287*, 1989–1992; c) J. A. Christodoulides, Y. Huang, Y. Zhang, G. C. Hadjipanayis, I. Panagiotopoulos, D. Niarchos, *J. Appl. Phys.* **2000**, *87*, 6938–6940; d) J.-I. Park, M. G. Kim, Y.-W. Jun, J. S. Lee, W.-R. Lee, J. Cheon, *J. Am. Chem. Soc.* **2004**, *126*, 9072–9078; e) S. R. Nicewarner-Peña, R. G. Freemann, B. D. Reiss, L. He, D. J. Peña, I. D. Walton, R. Cromer, C. D. Keating, M. J. Natan, *Science* **2001**, *294*, 137–141.
- [4] a) Z. Zheng, H. Li, T. Liu, R. Cao, *J. Catal.* **2010**, *270*, 268–274; b) S.-J. Kim, S.-D. Oh, S. Lee, S.-H. Choi, *J. Ind. Eng. Chem.* **2008**, *14*, 449–456; c) S. Koh, P. Strasser, *J. Am. Chem. Soc.* **2007**, *129*, 12624–12625; d) K. Sasaki, H. Naohara, Y. Cai, Y. M. Choi, P. Liu, M. B. Vukmirovic, J. X. Wang, R. R. Adzic, *Angew. Chem. Int. Ed.* **2010**, *49*, 8602–8607; *Angew. Chem.* **2010**, *122*, 8784–8789; e) V. R. Stamenkovic, B. Fowler, B. S. Mun, G. Wang, P. N. Ross, C. A. Lucas, N. M. Markovic, *Science* **2007**, *315*, 493–497.
- [5] a) Y. Lu, W. Chen, *ACS Catal.* **2012**, *2*, 84–90; b) E.-Y. Ko, E. D. Park, H. C. Lee, D. Lee, S. Kim, *Angew. Chem. Int. Ed.* **2007**, *46*, 734–737; *Angew. Chem.* **2007**, *119*, 748–751.
- [6] a) L. Prati, A. Villa, F. Porta, D. Wang, D. Su, *Catal. Today* **2007**, *122*, 386–390 and references 2, 8–11 therein; b) D. I. Enache, J. K. Edwards, P. Landon, B. Solsona-Espriu, A. F. Carley, A. A. Herzing, M. Watanabe, C. J. Kiely, D. W. Knight, G. J. Hutchings, *Science* **2006**, *311*, 362–365; c) J. K. Edwards, B. E. Solsona, P. Landon, A. F. Carley, A. Herzing, C. J. Kiely, G. J. Hutchings, *J. Catal.* **2005**, *236*, 69–79.
- [7] a) A. K. Singh, Q. Xu, *ChemCatChem* **2013**, *5*, 652–676; b) J. Shi, *Chem. Rev.* **2013**, *113*, 2139–2181.
- [8] a) H.-L. Jiang, Q. Xu, *J. Mater. Chem.* **2011**, *21*, 13705–13725; b) D. A. Hansgen, D. G. Vlachos, J. G. Chen, *Nat. Chem.* **2010**, *2*, 484–489; c) H. Kobayashi, M. Yamauchi, H. Kitagawa, Y. Kubota, K. Kato, M. Takata, *J. Am. Chem. Soc.* **2010**, *132*, 5576–5577; d) F. Studt, F. Abild-Pedersen, T. Bligaard, R. Z. Sørensens, C. H. Christensen, J. K. Nørskov, *Science* **2008**, *320*, 1320–1322.
- [9] S. Nishimura, Y. Yakita, M. Katayama, K. Higashimine, K. Ebitani, *Catal. Sci. Technol.* **2013**, *3*, 351–359.
- [10] I. Notar Francesco, F. Fontaine-Vive, S. Antonietti, *ChemCatChem* **2014**, *6*, 2784–2791.
- [11] a) J. Zhang, L. Zhang, Y. Jia, G. Chen, X. Wang, Q. Kuang, Z. Xie, L. Zheng, *Nano Res.* **2012**, *5*, 618–629; b) M. Chen, D. Kumar, C.-W. Yi, D. W. Goodman, *Science* **2005**, *310*, 291–293; c) J. Xu, T. White, P. Li, C. He, J. Yu, W. Yuan, Y.-F. Han, *J. Am. Chem. Soc.* **2010**, *132*, 10398–10406.
- [12] S.-B. Wang, W. Zhu, J. Ke, M. Lin, Y.-W. Zhang, *ACS Catal.* **2014**, *4*, 2298–2306.
- [13] a) D. Wang, Y. Li, *J. Am. Chem. Soc.* **2010**, *132*, 6280–6281; b) S. Maksimuk, S. Yang, Z. Peng, H. Yang, *J. Am. Chem. Soc.* **2007**, *129*, 8684–8685; c) Z. Peng, H. Yang, *Nano Today* **2009**, *4*, 143–164; d) L. Zhang, J. Zhang, Q. Kuang, S. Xie, Z. Jiang, Z. Xie, L. Zheng, *J. Am. Chem. Soc.* **2011**, *133*, 17114–17117.
- [14] a) S. N. Tripathi, S. R. Bharadwaj, M. S. Chandransekharaiyah, *J. Phase Equilib.* **1996**, *17*, 362–365; b) S. N. Tripathi, S. R. Bharadwaj, S. R. Dharwadkar, *J. Phase Equilib.* **1993**, *14*, 638–642.
- [15] a) K. Kusada, M. Yamauchi, H. Kobayashi, H. Kitagawa, Y. Kubota, *J. Am. Chem. Soc.* **2010**, *132*, 15896–15898; b) K. Kusada, H. Kobayashi, R. Ikeda, Y. Kubota, M. Takata, S. Toh, T. Yamamoto, S. Matsumura, N. Sumi, K. Sato, K. Nagaoka, H. Kitagawa, *J. Am. Chem. Soc.* **2014**, *136*, 1864–1871.
- [16] D. Wu, M. Cao, M. Shen, R. Cao, *ChemCatChem* **2014**, *6*, 1731–1736.
- [17] C. Huang, X. Yang, H. Yang, P. Huang, H. Song, S. Liao, *Appl. Surf. Sci.* **2014**, *315*, 138–143.
- [18] a) R. N. Dhital, H. Sakurai, *Chem. Lett.* **2012**, *41*, 630–632; b) J. Xiang, P. Li, H. Chong, L. Feng, F. Fu, Z. Wang, S. Zhang, M. Zhu, *Nano Res.* **2014**, *7*, 1337–1343; c) S. U. Son, Y. Jang, J. Park, H. B. Na, H. M. Park, H. J. Yun, J. Lee, T. Hyeon, *J. Am. Chem. Soc.* **2004**, *126*, 5026–5027.
- [19] a) M. Chen, Z. Zhang, L. Li, Y. Liu, W. Wang, J. Cao, *RSC Adv.* **2014**, *4*, 30914–30922; b) G. M. Scheuermann, L. Rumi, P. Steurer, W. Bannwarth, R. Mülhaupt, *J. Am. Chem. Soc.* **2009**, *131*, 8262–8270; c) Á. Molnár, *Chem. Rev.* **2011**, *111*, 2251–2320; d) N. Miyaura, A. Suzuki, *Chem. Rev.* **1995**, *95*, 2457–2483; e) J. A. Gladysz, *Pure Appl. Chem.* **2001**, *73*, 1391–1324.
- [20] a) R. Narayanan, *Molecules* **2010**, *15*, 2124–2138; b) M.-R. Kim, S.-H. Choi, *J. Nanomater.* **2009**, *2009*, 302919.
- [21] a) C. Boissiere, D. Grosso, A. Chaumonot, L. Nicole, C. Sanchez, *Adv. Mater.* **2011**, *23*, 599–623; b) D. P. Debecker, P. H. Mutin, *Chem. Soc. Rev.* **2012**, *41*, 3624–3650; c) G. A. Somorjai, J. Y. Park, *Angew. Chem. Int. Ed.* **2008**, *47*, 9212–9228; *Angew. Chem.* **2008**, *120*, 9352–9368.
- [22] a) N. Hoshiya, M. Shimoda, H. Yoshikawa, Y. Yamashita, S. Shuto, M. Arisawa, *J. Am. Chem. Soc.* **2010**, *132*, 7270–7272; b) L. D. Pachón, G. Rothenberg, *Appl. Organomet. Chem.* **2008**, *22*, 288–299; c) M. B. Thathagar, J. E. ten Elshof, G. Rothenberg, *Angew. Chem. Int. Ed.* **2006**, *45*, 2886–2890; *Angew. Chem.* **2006**, *118*, 2952–2956; d) A. V. Gaikwad, A. Holuique, M. B. Thathagar, J. E. ten Elshof, G. Rothenberg, *Chem. Eur. J.* **2007**, *13*, 6908–6913.
- [23] a) C. D. Wanger, W. M. Riggs, L. E. Davis, J. Moulder, in *Handbook of X-ray Photoelectron Spectroscopy-A Reference Book of Standard Data for Use in X-ray Photoelectron Spectroscopy*, PerkinElmer Corporation, Physical Electronic Division, Minnesota, **1979**, pp. 8–11 and pp. 110–111; b) J. M. Tura, P. Regull, L. Victori, M. D. de Castellar, *Surf. Interface Anal.* **1988**, *11*, 447–449; c) M. M. Coulter, J. A. Dinglasan, J. B. Goh, S. Nair, D. J. Anderson, V. M. Dong, *Chem. Sci.* **2010**, *1*, 772–775; d) J. Y. Shen, A. Adnot, S. Kaliaguine, *Appl. Surf. Sci.* **1991**, *51*, 47–60.
- [24] J. A. Rodriguez, D. W. Goodman, *Science* **1992**, *257*, 897–903.
- [25] a) P. J. Feibelman, D. R. Hamann, *Phys. Rev. Lett.* **1984**, *52*, 61; b) L. M. Falicov, G. A. Somorjai, *Proc. Natl. Acad. Sci. USA* **1985**, *82*, 2207–2211; c) M. H. Cohen, M. V. Ganduglia-Pirovano, J. Kudrnovský, *Phys. Rev. Lett.* **1994**, *72*, 3222; d) J. Harris, S. Andersson, *Phys. Rev. Lett.* **1985**, *55*, 1583.
- [26] C. Q. Sun, Y. Wang, Y. G. Nei, B. R. Mehta, M. Khanuja, S. M. Shivaprasad, Y. Sun, J. S. Pan, L. K. Pan, Z. Sun, *Phys. Chem. Chem. Phys.* **2010**, *12*, 3131–3135.
- [27] E. Nikolla, J. Schwank, S. Linic, *J. Am. Chem. Soc.* **2009**, *131*, 2747–2754.
- [28] Y. Na, S. Park, S. B. Han, H. Han, S. Ko, S. Chang, *J. Am. Chem. Soc.* **2004**, *126*, 250–258.
- [29] S. Proch, Y. Mei, J. M. R. Villanueva, Y. Lu, A. Karpov, M. Ballauff, R. Kempe, *Adv. Synth. Catal.* **2008**, *350*, 493–500.
- [30] a) S. Saito, S. Oh-tani, N. Miyaura, *J. Org. Chem.* **1997**, *62*, 8024–8030; b) C. M. Nunes, A. L. Monterio, *J. Braz. Chem. Soc.* **2007**, *18*, 1443–1447.
- [31] P. K. Mandal, D. K. Chand, *Catal. Commun.* **2013**, *31*, 16–20.
- [32] a) P. J. Ellis, I. J. S. Fairlamb, S. F. J. Hackett, K. Wilson, A. F. Lee, *Angew. Chem. Int. Ed.* **2010**, *49*, 1820–1824; *Angew. Chem.* **2010**, *122*, 1864–1868; b) Z. Niu, Q. Peng, Z. Zhuang, W. He, Y. Li, *Chem. Eur. J.* **2012**, *18*, 9813–9817; c) Ö. Metin, S. F. Ho, C. Alp, H. Can, M. N. Mankin, M. S. Gültekin, M. Chi, S. Sun, *Nano Res.* **2013**, *6*, 10–18; d) Y. Wu, D. Wang, P. Zhao, Z. Niu, Q. Peng, Y. Li, *Inorg. Chem.* **2011**, *50*, 2046–2048.
- [33] F. González de Rivera, I. Angurell, M. D. Rossell, R. Erni, J. Llorca, N. J. Divins, G. Muller, M. Seco, O. Rossell, *Chem. Eur. J.* **2013**, *19*, 11963–11974.
- [34] a) Y. M. A. Yamada, S. M. Sarkar, Y. Uozumi, *J. Am. Chem. Soc.* **2012**, *134*, 3190–3198; b) P. M. Uberman, L. A. Pérez, G. I. Laccioni, S. E. Martin, *J. Mol. Catal. A* **2012**, *363–364*, 245–253.
- [35] J. P. Corbet, G. Mignani, *Chem. Rev.* **2006**, *106*, 2651–2710.

Received: July 7, 2015

Revised: August 7, 2015

Published online on October 5, 2015